Case Studies in Thermal Engineering 28 (2021) 101675

Contents lists available at ScienceDirect

Case Studies in Thermal Engineering

journal homepage: www.elsevier.com/locate/csite

Effect of magnetic field on heat transfer from a channel: Nanofluid flow and porous layer arrangement

Somayeh Davoodabadi Farahani [a,*], Mohammad Amiri [a], Behnam Kazemi Majd [a], Amir Mosavi [b,c,**]

[a] School of Mechanical Engineering, Arak University of Technology, 38181-41167, Arak, Iran
[b] John von Neumann Faculty of Informatics, Obuda University, Budapest, Hungary
[c] Institute of Information Society, University of Public Service, 1083 Budapest, Hungary

ARTICLE INFO

Keywords:
Shape of a porous layer
Central and boundary arrangement
Nanofluid
Magnetic field
Heat transfer

ABSTRACT

Due to the high number of porous media applications in industries, the demands for analyzing the porous medium's flow and heat transfer are rising every day. The present research intends to evaluate the impact of porous media, nanofluid, and magnetic field on heat transfer of a circular channel. Two typical porous arrangements are considered: central configuration and boundary configuration. It is of interest to know the impact of porosity, thickness, permeability, and thermal conductivity ratio in porous media. The working fluid, nanoparticles and porous medium are water, CuO and steel foam, respectively. The results reveal that the heat transfer rate in the central arrangement is more than the boundary arrangement. When the non-dimensional thickness of the porous media is 0.8 in the central arrangement, the heat transfer rate is at its peak. Simultaneously, the minimum happens when the non-dimensional thickness is set to 0.6 in the boundary arrangement. Applying nanofluid and increasing the volume fraction will improve the heat transfer rate. The average heat transfer coefficient is increased when the magnetic field is applied up to the intensity of 0.5 T. Additionally, the maximum heat transfer enhancement is achieved when the thickness is 0.6 in boundary arrangement in the case of applying the magnetic field, which is estimated to be 3–5% more. Modifying the shape of the porous media in the boundary arrangement decreases the heat transfer rate about 7–21%, depending on the shape compared to a homogeneous boundary porous.

1. Introduction

Investigating the thermal behavior and flow field within porous material is a relatively old topic in heat transfer and fluid mechanics. The porous media is used in industries such as thermal insulation technology, heat exchangers design, casting industries, and many others [1]. To this end, many various models are introduced with the purpose of simulating the flow field and heat transfer within porous media precisely [2]. Darcy's law is one of the prevalent models that is used widely. Horkheimer's porous-media flow model was subsequently presented in which the additional nonlinear drag force was able to refine the simulation of the flow in high velocities. Furthermore, the Brinkman form of Darcy's law was presented later. The additional term of viscous stress succeeded in implementing the no-slip condition in the solid matrix, and the boundary layer's effect was also brought into the momentum equation.

* Corresponding author.
** Corresponding author. John von Neumann Faculty of Informatics, Obuda University, Budapest, Hungary.
E-mail addresses: sdfarahani@arakut.ac.ir (S.D. Farahani), amir.mosavi@kvk.uni-obuda.hu (A. Mosavi).

https://doi.org/10.1016/j.csite.2021.101675
Received 13 June 2021; Received in revised form 29 October 2021; Accepted 26 November 2021
Available online 27 November 2021

Darcy's law, Forchheimer's porous-media flow model, and the Brinkman form of Darcy's law are the standard models widely employed to solve the flow field through porous media in many numerical studies [3]. Nithiarasu et al. [4] investigated the natural convective heat transfer and flow field in a fluid-saturated variable porosity medium using Brinkman-Forchheimer model. Based on their findings, increasing the Darcy number, which is followed by an increase in the velocity, makes it possible to neglect the share of shape effects on drag forces against viscous drag. In some industrial applications, such as casting process control of some parts with desired properties and thermal insulation technology for energy saving purposes, the system includes a 2D domain where layers of porous media are in contact with the layers of fluid. The walls in the top and bottom boundaries are insulated, and the side walls are at a constant temperature [5,6].

Many numerical studies are conducted utilizing Darcy's law, Brinkman-Forchheimer, and specifically, the Brinkman form of Darcy's law to examine porous media's effect on the flow field as well as the thermal behavior in various arrangements [7]. In the field of flow modeling and heat transfer in a chamber with a porous layer, we can refer to the study of Beckerman et al. [8].

Baragh et al. [9] experimentally examined the forced convection heat transfer of air in a channel featuring different configurations of porous material in the form of circular surfaces in the core of the channel. The results demonstrate that as the porous diameter and the airflow rate rise, the maximum heat transfer rate is obtained. The temperature rise will decline the temperature difference between the walls and the fluid's average temperature. Nimvari and Jouybari [10] examined the impact of turbulence on the thermal behavior of a pipe partly filled with porous media. As they reported, the turbulence effect is more influential in selecting porous media thickness compared to the laminar flow since more flow passes through the porous media. Shokouhmand et al. [11] studied the thermal dispersion effects on convective heat transfer of gas in laminar flow in a microtube filled with a spongy material. Their reports show that increasing the humidity effect has a negative impact on thermal behavior. Increasing Nusselt number becomes crucial due to dispersion in low Biot number where conduction heat transfer occurs, but it can be neglected in higher Biot numbers. Peng et al. [12] explored the thermal conduction effect within a porous media on Nusselt number and heat exchangers performance. Laminar flow within the fully developed region and central arrangement of the porous media is defined as their research's assumptions. The

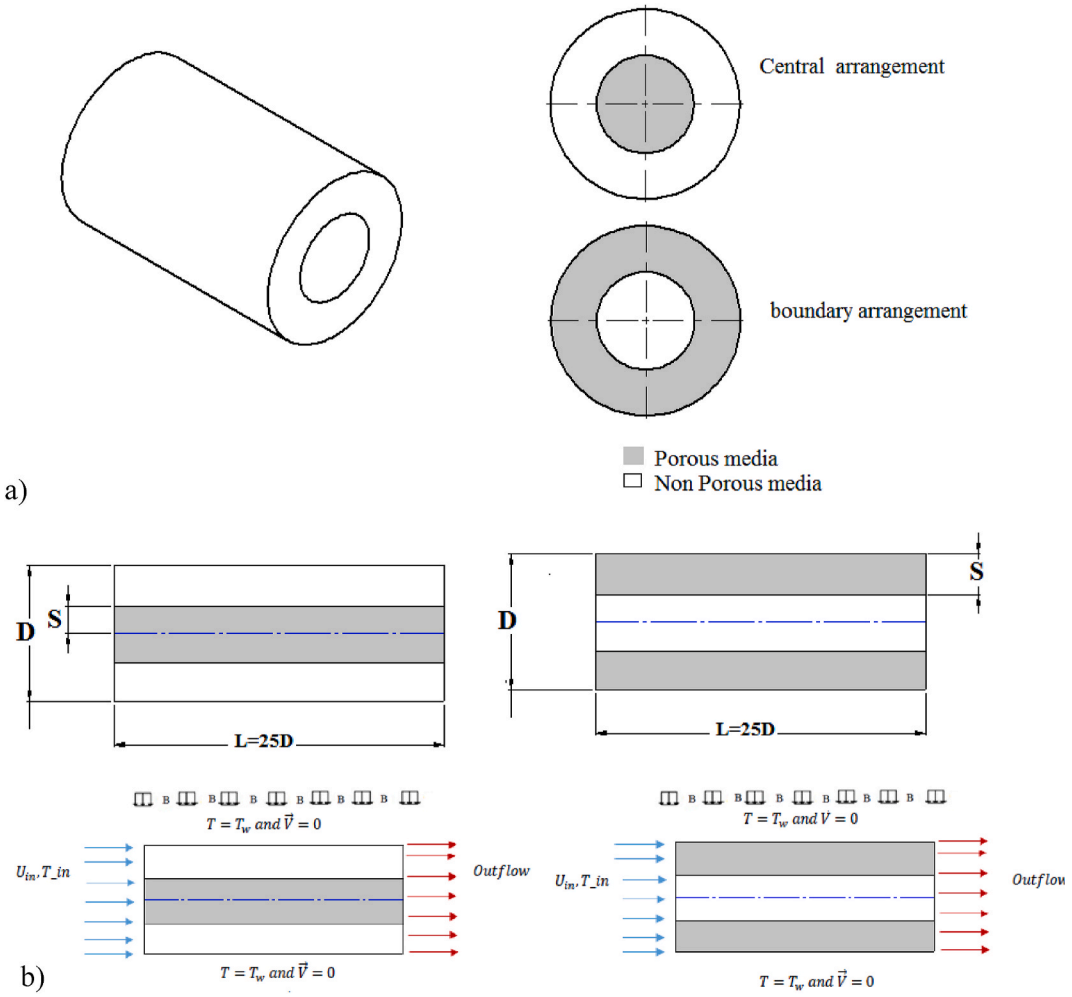

Fig. 1. a) Geometry of the problem with dimensions, and b) boundary conditions.

numerical simulation was conducted with four different cases; Two cases with air, one with water, and one with a fluid with the relative density of ¼ (water is the reference substance). The porosity, Reynolds number, and the porous media' thermal conductivity are set to 0.9, 25–2000, and 0.1–200, respectively. Their findings show that increasing the porous media's thermal conductivity does not consistently increase the Nusselt number and performance criteria. Zheng et al. [13] offered a contemporary method for optimizing the thermal behavior in a tube partly filled with a porous material. Their approach is based on the genetic algorithm and CFD, which are used simultaneously. Their results show that several porous layers with various porosity can multiply the heat transfer rate. Dehghan et al. [14]examined the thermal conductivity effect on the developed convective flow through two parallel flat surfaces occupied with porous media. According to their analytical results, the Nusselt number increases semi-linearly in case of a linear increase in porous media's thermal conductivity. Wang et al. [15] presented an innovative methodology for thermal enhancement and pressure drop reduction through a channel partially filled with both homogenous and inhomogeneous porous media. A constant temperature boundary condition is considered for the wall. Based on their results, at the radius of 0.6 and 1, the corresponding Nusselt number increases, and the pressure drop is pretty small.

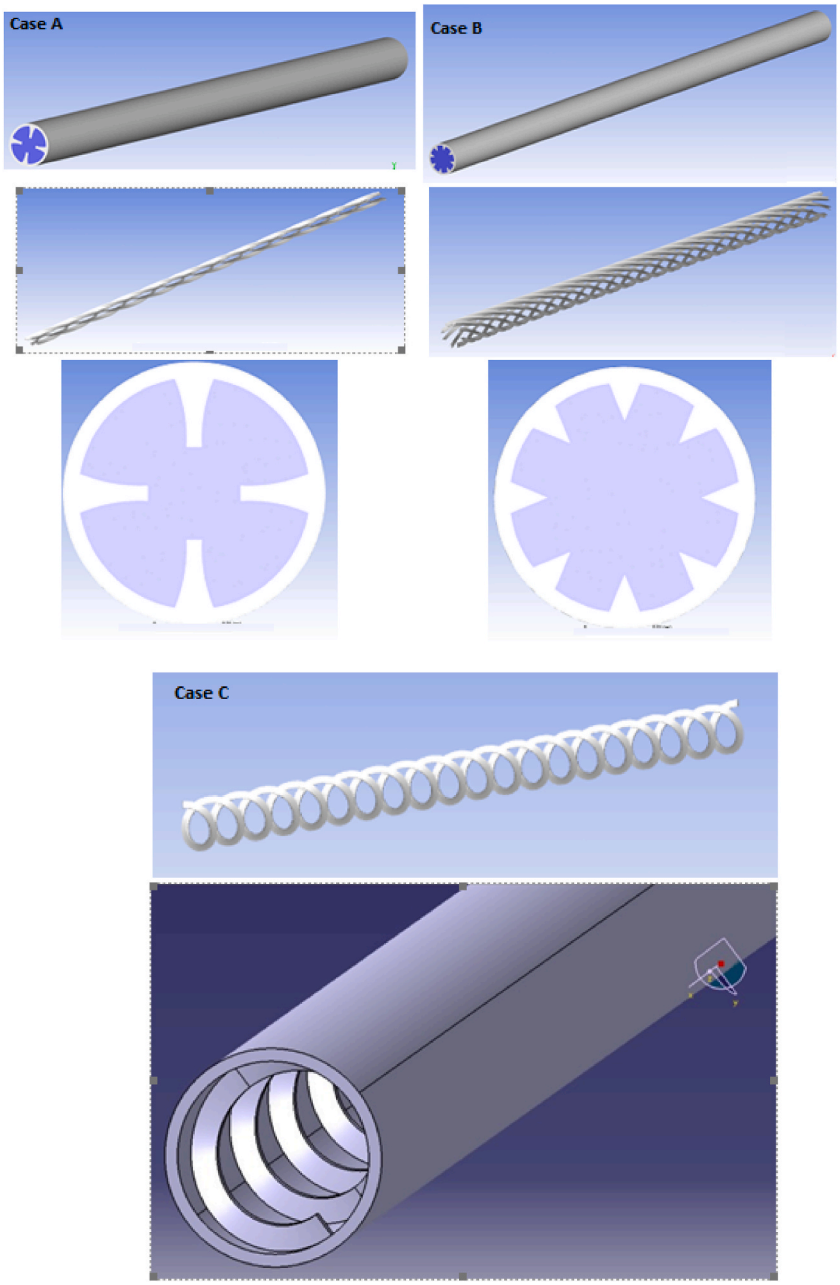

Fig. 2. Geometries of cases A, B, and C.

There are also many experimental and numerical studies regarding nanofluid's effect on natural and forced convective heat transfer enhancement [16–20]. For instance, Al-Rashed [21] carried out 3D-analytical research concerning magneto-convective heat transfer in an enclosed environment. Their findings indicate that the magnetic field's placement is particularly important when investigating the thermal characteristics. Sheikholeslami et al. [22] examined the forced convection heat transfer of Fe_3O_4–water nanofluid exposing to a magnetic field. In another research [23], a similar approach was followed for a porous environment. They found out that increasing the nanoparticles increases Lorentz force. Selimefendigil et al. [24] investigated the magnetic field effect on mixed convection of Al_2O_3–water nanofluid. There are other studies in the field of fin on heat transfer [25], porous fin [26] and nanofluid [27].

Regarding the papers reviewed, the non-uniform magnetic field effect on heat transfer of a channel incompletely filled with the porous medium has not been given much attention despite all the research carried out. Two typical porous arrangements are considered for this study; the central arrangement in which the porous region is situated in the channel's core and the boundary arrangement where the porous media is affixed to the channel's wall. Thus, the present research aims to study the thermal behavior of a nanofluid in a pipe occupied with porous media featuring a non-uniform magnetic field. The corresponding parameters to the porous media, including thickness, permeability, porosity, thermal conductivity ratio, and porous arrangement, are evaluated. The research involves a 3D simulation utilizing Finite Volume Method (FVM) and the multiphase model to simulate the nanofluid.

2. Mathematical model and governing equations

The current study deals with the effect of porous media and the non-uniform magnetic field of a nanofluid through a pipe. A 3D-channel with a circular cross-section is modeled. Two arrangements are assumed for the porous region in this problem; the central arrangement in which the porous zone is situated in the channel's core and the boundary arrangement where the porous media is affixed to the channel's wall. Fig. 1 illustrates the problem's geometry. Additionally, other porous shapes are considered for boundary arrangements to examine how different shapes of porous affect the results, as shown in Fig. 2. The length of the fins is assigned with S, and the twisting pitch is 400 mm. Assuming a laminar, incompressible, and steady flow at the inlet, momentum, continuity, and energy equations [14] outside of the porous region are formulated as follow:

$$\nabla.(\rho.V) = 0 \tag{1}$$

$$\rho V.\nabla V = -\nabla P + \nabla.(\mu \nabla V) \tag{2}$$

$$\rho V.\nabla T = \nabla.(k.\nabla T) \tag{3}$$

Where ρ, μ, k, P, V and T are density, dynamic viscosity, thermal conductivity, pressure, velocity, and temperature, respectively. The porous media in this research is assumed to be an artificial saturated homogenous kind in which the permeability is equal in all directions. Permeability is independent of fluid and is most likely a function of the mean size, shape, and particle density of the porous media particles. Spherical stainless-steel particles with a diameter of 0.605 mm constitute the porous environment components. The radiation heat transfer is neglected from porous media. The porosity of the porous region and the fluid thermophysical properties are assumed to be constant. The solid phase is in thermal equilibrium with the fluid phase of the flow that is a valid presumption for low Darcy and Reynolds numbers. It is also assumed that the walls are in no-slip condition. The upstream flow is considered to be a one-dimensional flow along the pipe axis at a constant velocity and uniform temperature. The continuity, momentum, and energy equations through porous media [2] are defined as follow:

$$\overrightarrow{\nabla}.\left(\varepsilon \rho_f \overrightarrow{V}\right) = 0 \tag{4}$$

$$\rho_f \left(\overrightarrow{V}.\nabla\right)\overrightarrow{V} = \varepsilon^2 \left(\overrightarrow{\nabla} P - \left(\frac{\mu_f}{K} + \frac{\rho_f C}{\sqrt{K}}\left|\overrightarrow{V}\right|\right)\overrightarrow{V} + \frac{\mu_f}{\varepsilon}\nabla^2 \overrightarrow{V}\right) \tag{5}$$

$$\left(\rho_f C_f + \frac{1-\varepsilon}{\varepsilon}\rho_s C_s\right)\overrightarrow{V}.\overrightarrow{\nabla} T = \left(k_f + \frac{1-\varepsilon}{\varepsilon}k_s\right)\nabla^2 T \tag{6}$$

Where V، ε, ρ_s، ρ_f ،μ_f, C_s, C_f، C، P ،K, k_f ، k_s are defined as a velocity vector, porosity coefficient, density of the solid material, density of the fluid, fluid dynamic viscosity, the heat capacity of the solid and fluid, pressure, the permeability of the porous media, thermal conductivity of the fluid and solid material respectively. Forchheimer's constant [2] is given as follow:

$$C = \frac{1.75}{\sqrt{150 \times \varepsilon^5}} \tag{7}$$

The permeability of porous media means the capability of the material in carrying the fluid and is defined as follow [2]:

$$K = \frac{\varepsilon^2 Dp^2}{150(1-\varepsilon)^2} \tag{8}$$

Where Dp is the mean size of the particles. The nanofluid flow simulation is done with the help of the Mixture two-phase model when it is considered as the working fluid. The flow components, including the fluid and nanoparticles, are solved using the continuity,

momentum, and energy equations. It is also presumed that the relative velocity between the two phases can be both zero and non-zero. This approach assumes that the existing phases are in a continuous environment. An individual velocity vector is defined for every phase, and each control volume contains the corresponding volume fraction to each phase. Therefore, the continuity, momentum, energy, and volume fraction are specified as follow [28]:

$$\nabla.\left(\rho_{mi}\overrightarrow{V_{mi}}\right)=0 \tag{9}$$

$$\nabla.\left(\rho_{mi}\vec{V}_{mi}\ \vec{V}_{mi}\right)=-\nabla P+\nabla.\left(\mu_{mi}\nabla\vec{V}_{mi}\right)+\nabla.\left(\varnothing\rho_{p}\nabla\vec{V}_{dr,P}\nabla\vec{V}_{dr,P}\right) \tag{10}$$

$$\nabla.\left[\left(\phi\rho_{P}c_{P,P}\overrightarrow{V_{P}}+(1-\phi)\rho_{f}c_{P,f}\overrightarrow{V_{f}}\right)T\right]\ =\ \nabla.(k_{mi}\nabla\mathrm{T}) \tag{11}$$

$$\nabla.\left(\varnothing\rho_{P}\vec{V}_{mi}\right)=-\nabla.\left(\varnothing\rho_{P}\vec{V}_{dr,P}\right) \tag{12}$$

Where $\vec{V}_{mi}$ and $\vec{V}_{dr,P}$ are mean mass velocity and drift velocity, respectively. They are given below [28]:

$$\rho_{mi}\vec{V}_{mi}=\varnothing\rho_{p}\vec{V}_{p}+(1-\varnothing)\rho_{f}\vec{V}_{f} \tag{13}$$

$$\vec{V}_{dr,P}=\vec{V}_{p}-\vec{V}_{f}=\vec{V}_{pf} \tag{14}$$

Momentum and energy equations are modified for the magnetic field as follow [29]:

$$\rho\left(\vec{V}.\nabla\vec{V}\right)=-\vec{\nabla}\mathrm{P}+\mu\nabla^{2}\vec{V}+\rho\ \ \beta\ \vec{g}(\mathrm{T}-\mathrm{T_{re}})+\mu_{0}\left(\vec{M}.\nabla\right)\vec{B}+\vec{j}\times\vec{B} \tag{15}$$

$$\rho\mathrm{C}\vec{\mathrm{V}}.\nabla\mathrm{T}=k\nabla^{2}\mathrm{T}+\frac{\vec{j}^{2}}{\sigma_{m}} \tag{16}$$

Where $\mu_0, \mathrm{M}, \sigma_m,$ and B are assigned as magnetic permeability in vacuum condition, magnetism, electrical conductivity, and magnetic field intensity, respectively. The electric current intensity is given by $\vec{j}$ which is determined as follow:

$$J=\frac{\nabla\times B}{\mu_{B}} \tag{17}$$

Where μ_B is the magnetic permeability. M is defined using the following equation [29]:

$$\mathrm{M}=\frac{6m_{p}}{\pi\ d_{p}^{3}}\left\{\coth\left(\frac{\mu0m_{p}\ B}{K_{b}\ T}\right)-\frac{K_{b}\ T}{\mu0m_{p}\ B}\right\} \tag{18}$$

Where m_p, d_p, K_b are defined as magnetic momentum, the diameter of the magnetic particle, and Boltzmann constant, respectively. The non-uniform magnetic field generated by the electric current can be written as follow [29]:

$$\vec{B}=\frac{I}{2\pi\left((x-a)^{2}+(y-b)^{2}\right)}\left(-(y-b),(x-a)\right) \tag{19}$$

Where I and $(a,\ b)$ are the electric current intensity and its location. The magnetic field is generated with a specific voltage, and the corresponding current is determined using Ohm's law. Reynolds number and Darcy number are given as below [14]:

$$\mathrm{Re}=\frac{\rho_{\mathrm{f}}\mathrm{V_{inlet}}D}{\mu_{\mathrm{f}}} \tag{20}$$

$$\mathrm{Da}=\frac{\mathrm{K}}{\mathrm{D}^{2}} \tag{21}$$

Where V_{inlet}, *and* D are inlet velocity, and diameter of the channel, respectively. Nusselt number and convective heat transfer coefficient are determined using equations (22) and (23) [28]:

$$\mathrm{Nu}=\frac{\mathrm{hD}}{\mathrm{k_{f}}} \tag{22}$$

$$\mathrm{h}=\frac{-\mathrm{k_{f}}\frac{\partial\mathrm{T}}{\partial y_{\mathrm{channel's\,wall}}}}{\mathrm{T_{w}}-\mathrm{T_{m}}} \tag{23}$$

T_w and T_m are assigned as wall temperature and the mean fluid temperature, respectively. The constant temperature of $\boldsymbol{T_w}$ and no-slip condition are assumed as the boundary conditions for the solid wall, as illustrated in Fig. 1. The inlet flow is considered to be at a uniform temperature and velocity of $\boldsymbol{T_C}$ and $\boldsymbol{U_c}$. The outflow boundary condition is employed for the outlet as well. The magnetic field is exposed to the wall. The thermodynamic properties of the fluid and every other material are constant throughout the calculations. The base fluid is water and the nanoparticles used are copper oxide, CuO, with a diameter of 0.1 nm. The porous media is in the form of stainless-steel foam. Table 1 presents the properties corresponding to the materials. The flow field is solved numerically with the help of FVM. The energy and momentum equations are discretized with the second-order upwind model. The standard model was employed for the discretization of pressure. Velocity and pressure are coupled by utilizing the SIMPLE formula. Under relaxation factors are 0.3, 1, and 0.7 for pressure, density and momentum, respectively. With the existing assumptions and boundary conditions considered for the problem, the simulation is repeated with different grid numbers to achieve a precise solution and reduce the error caused by grid size. Fig. 3a indicates the changes of the average Nusselt number and velocity for air within Re = 20000 in the channel's center. The grid with 2500000 elements is chosen as the final grid to resume the analysis. Fig. 3b shows the organized mesh of the circular cross-section.

3. Validation

The validation involves comparing the results for Da = 1E-4, Re = 50, and porosity of 0.97 with the ones obtained by Baragh et al. [9]. Fig. 4a and b demonstrate the changes of the Nusselt number with the thickness. The results differ by approximately less than 6%, which indicates the precision of the study. It is vital to take into account the fact that the relevant reference was conducted in 2D space. Another validation is performed for a model in which the porous region is placed close to the wall for turbulent flow [30]. According to the results illustrated in Fig. 4c, the error is estimated to be 10%. Generally, the validations demonstrate the precision of the numerical study.

4. Results

The influence of various configurations of porous media, magnetic field, nanofluid, and porous shape are examined. Fig. 5a displays the efficacy of thickness on the velocity profile for Da = 1E-4, $\varepsilon = 0.8$, and Re = 20000 in the central arrangement. It can be illustrated that increasing the thickness drives the fluid from the porous portion into the non-porous zone and increases the velocity gradient between the wall and porous media. Accordingly, increasing the thickness results in an increase in maximum velocity, which is continued up to the thickness of 0.8. Fig. 5b illustrates Nusselt number's changes with the porous media's thickness along the channel's length. It is evident that the Nusselt number behaves the same as the velocity. Increasing the thickness of the porous zone raises *Nu* noticeably comparing to the non-porous one. Such thermal behavior is in connection with the fact that enlarging the porous portion across the pipe drives more fluid into the non-porous region. Furthermore, the maximum velocity magnitude and the velocity gradient increase at a distance near to the wall. Increasing the porous media thickness reduces the Nusselt number for thicknesses more than 0.8 compared to the non-porous case. Reduction of the Darcy number is meant to reduce the porous media's permeability, which increases the resistance and avoids flowing more fluid within the porous region. Therefore, the extra fluid has no other way to travel but the vacant space between the wall and porous media. The maximum velocity is increased in the non-porous zone, followed by reducing the thickness of the boundary layer; Fig. 5c shows these changes for Re = 20000, $\varepsilon = 0.8$, and $S = 0.8$.

Fig. 5d illustrates the Darcy number effect on Nusselt number along the channel for Re = 20000, $\varepsilon = 0.8$, and $S = 0.8$. Reducing the Darcy number slows down the fluid from moving within the porous zone and has no other way but the vacant space between the wall and porous media. The velocity gradient close to the wall augments and the *Nu* is expected to increase according to the Reynolds analogy. The porous layer's effect in the boundary arrangement for Da = 1E-4, $\varepsilon = 0.8$, and thickness of 0.8 is illustrated in Fig. 6a. The velocity variation with the porous layer thickness in this arrangement is the same as the central arrangement. The fluid is most likely to move in the non-porous portion because of the porous media's resistance. Just like what is discussed for central arrangement, the velocity increment is observed up to a specific thickness. The Nusselt number's variation with various thicknesses in boundary arrangement is shown in Fig. 6b. Affixing a coat of porous material to the pipe's inner wall forces the fluid to move through the center of the pipe; thus, the fluid velocity reduces through the porous media, resulting in the reduction of the fluid flow and velocity gradient near the wall. Accordingly, the Nusselt number is reduced until a specific thickness where the minimum Nusselt number occurs. The thicker the porous layer is, the lower the velocity gradient near the wall, which can reduce the Nusselt number; however, this is valid for the thickness equal to or less than 0.6. The temperature gradient and *Nu* begins to decline with increasing the thickness of more than 0.6. There is a point for thickness 0.6, where the heat transfer rate is minimum in the boundary arrangement. Fig. 6c indicates that decreasing the Darcy number reduces the permeability so that less fluid flow is seen within the porous zone in boundary arrangement. The velocity gradient in the porous-nonporous region increases with decreasing Darcy number. The variation of Nusselt number along

Table 1
Thermophysical properties of materials [14].

Material	$\rho\left(\frac{kg}{m^3}\right)$	$C_p\left(\frac{J}{kgK}\right)$	$k\left(\frac{W}{mK}\right)$	$\mu(Pa.s)$
Pure water	998.2	4182	0.6	0.000855
stainless steel foam	8030	8030	16.27	_
Cuo	6500	540	18	_

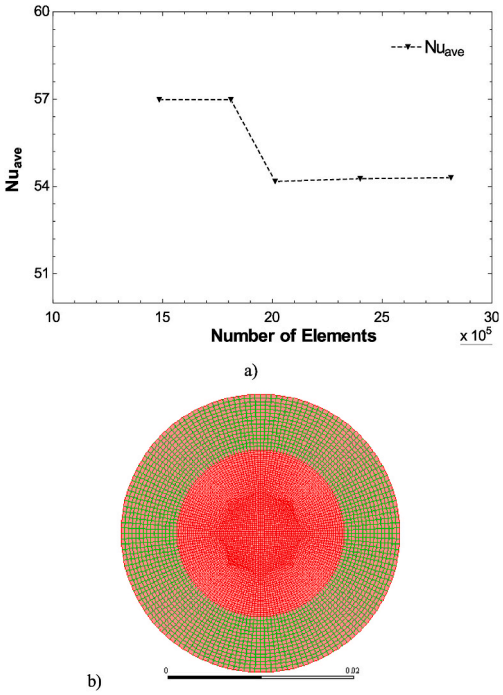

Fig. 3. a) Grid independency study, and b) A sample of an organized mesh of the cross-section of the channel.

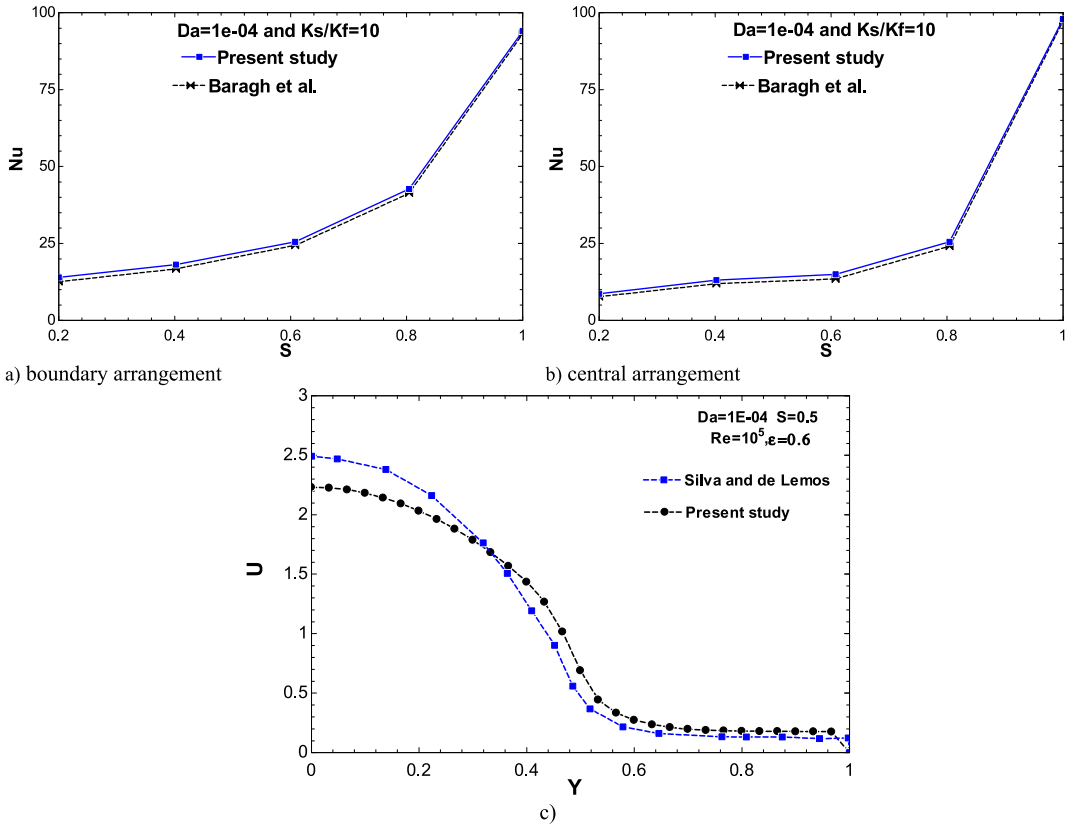

Fig. 4. Validation of the study by comparing the Nusselt number for various thickness of porous media a) for boundary arrangement, b) for central arrangement, and c) velocity distribution in the center of the channel for turbulent flow.

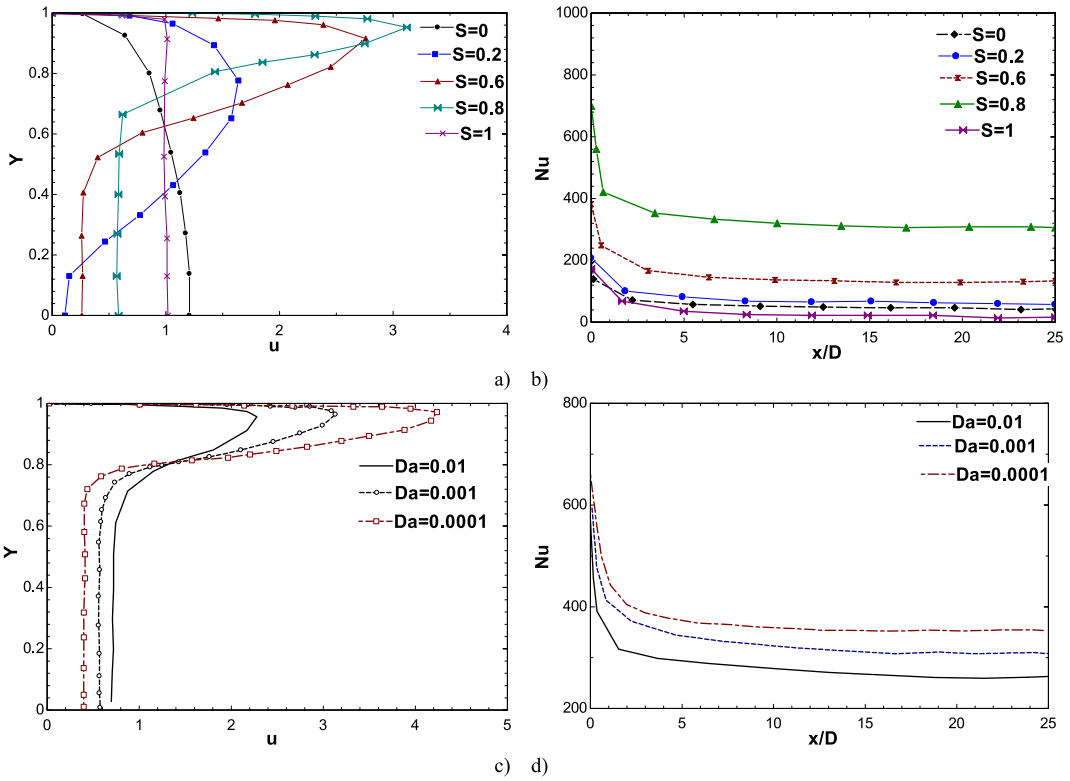

Fig. 5. a) Velocity profile at Da = 1E-4, ε = 0.8, and Re = 20000, for central arrangement b) variation of the local Nusselt number with various thicknesses for the central arrangement along the channel's length at Da = 1E-4, c) variation of the velocity profile with Darcy number at S = 0.8, ε = 0.8, and Re = 20000, for the central arrangement, and d) variation of the local Nusselt number with various Darcy numbers for the central arrangement along the channel's length at S = 0.8.

the channel for different Darcy numbers in the boundary arrangements is indicated in Fig. 6d. The Nusselt number is increased in the case of increasing the Darcy number because more fluid flows near the wall. It can be deduced that the heat transfer rate is higher in the central arrangement than the boundary arrangement. The impact of thermal conductivity ratio (K_s/K_f) on the convective heat transfer coefficient is studied for boundary arrangement, and the results are shown in Fig. 7a. The porosity of the porous media and Reynolds number are considered to be 0.8 and 20000, respectively. The averaged *Nu* rises with increasing K_s/K_f for every Darcy number. Additionally, the heat transfer rate is estimated to increase by 32% when the thermal conductivity ratio changes from 0.5 to 10. Fig. 7b shows nanofluid particles' impact on the heat transfer coefficient for the boundary configuration at Da = 1E-4, ε = 0.8, and Re = 20000. Increasing the nanofluid volume fraction causes the average *Nu* to grow regardless of the porous layer's thickness. It is also evident that the higher effective thermal conductivity of the nanofluid results in a more uniform temperature distribution along the channel (Fig. 7c). Moreover, the heat transfer rate is improved when the temperature gradient increases near the wall. The lowest rise of the heat transfer coefficient occurs when the thickness of the porous media is 0.6. The incline of the velocity profile for $S = 0.6$ is less than the others, followed by a decline in Nusselt number based on the Chilton-Colburn analogy. Altogether, the average heat transfer coefficient increase is estimated to be 0.8–12% when using nanofluid particles.

Fig. 7d demonstrates the heat transfer coefficient variation with different porosities at Da = 1E-4, Re = 20000, S = 0.2, and $\varphi = 5\%$. With an eye on the data shown in Fig. 7d, the convective heat transfer coefficient rises as the porosity grows, which is approximated to be 1%, 4.5%, 5.5%, and 11.1% for porosities equal 0.6, 0.7, 0.8, and 0.9, respectively compared to the base case. In the case without nanoparticles, the volume of fluid in the porous portion increases with increasing porosity coefficient. The temperature gradient on the channel wall decreases, and the convection heat transfer coefficient decreases. The fluid's thermal conductivity in the porous zone is increased when the nanoparticles are applied to the base fluid, which increases the temperature gradient on the wall. Finally, the convection heat transfer coefficient increases. Additionally, increasing the porosity coefficient reinforces the positive effect of using nanoparticles on the pipe's thermal behavior.

The variations of the heat transfer coefficient with the magnetic field are illustrated in Fig. 8a. The case is configured for the boundary arrangement at Da = 1E-4, ε = 0.8, Re = 20000, $\varphi = 5\%$, and S = 0.6. With respect to Fig. 8a, the average convective heat transfer rises with increasing the magnetic field intensity up to 0.5 T. Then it falls following the further increment of the magnetic field intensity. Such behavior is due to changes caused by the magnetic field in the flow pattern, which generates three regions, including the core, Hartman layer, and side layer in the channel. The shear stress near the wall is so intense that the shear force can compete with the Hartman layer's magnetic force near the wall. Inertial and shear forces are negligible, and the velocity magnitude is almost zero in the core zone. The velocity magnitude is greater in the side layers than the two other layers. The combination of the velocity

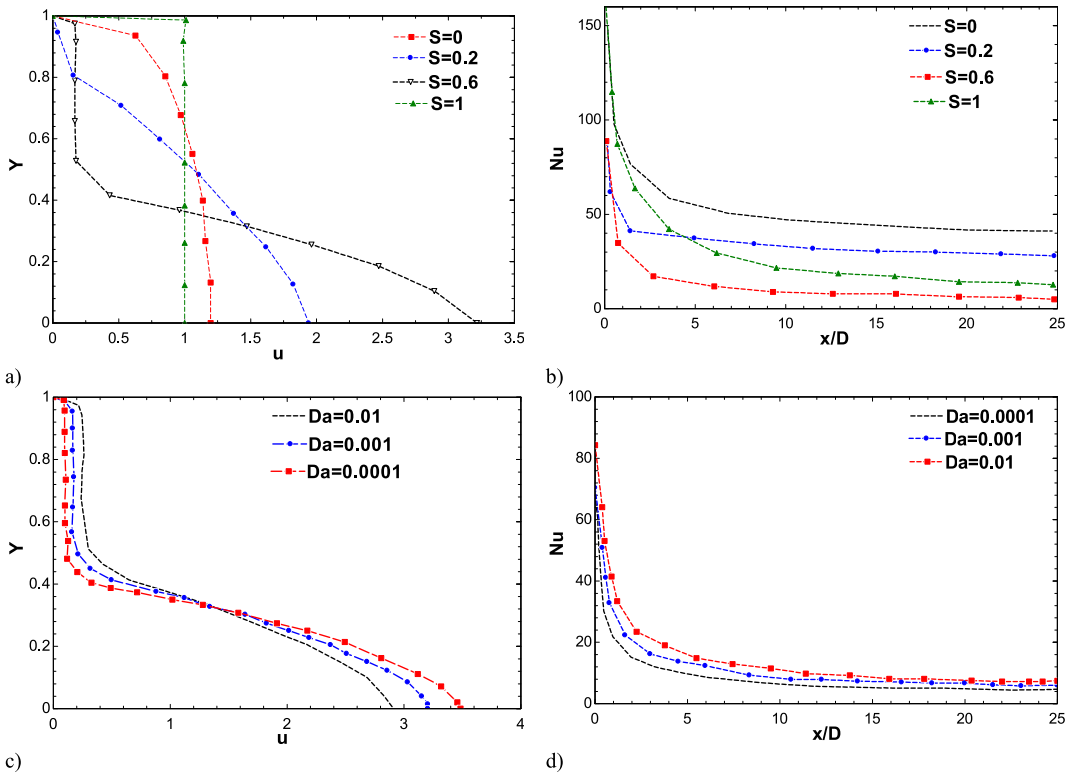

Fig. 6. a) Velocity profile at Da = 1E-4, ε = 0.8, and Re = 20000 for boundary arrangement, b) variation of the local Nusselt number with various thicknesses for boundary arrangement along the channel's length at Da = 1E-4, c) variation of the velocity profile with Darcy number at S = 0.8, ε = 0.8, and Re = 20000 for boundary arrangement, and d) variation of the local Nusselt number with various Darcy numbers for boundary arrangement along the channel's length S = 0.8.

distribution in these three regions creates a velocity profile, namely M shape, in the channel that can be spotted in Fig. 8a for magnetic field intensities more than 0.5 T. The efficacy of the magnetic field on the temperature field is indicated in Fig. 8c. It is noticeable that a more uniform temperature distribution results from increasing the magnetic field intensity from 0 to 0.5 T. The wall's temperature gradient rises as well; therefore, the heat transfer coefficient increases. The temperature gradient decreases if the magnetic field intensity is increased from 0.5 to 15 T, which results in a reduction of the convective heat transfer coefficient.

Fig. 8d gives information about the changes of the average heat transfer coefficient with *Re* for boundary arrangements at $\varphi =$ 5% *and* $\beta = 0.5$ *Tesla*. An external magnetic field causes the magnetic nanoparticles to be attracted to the wall and increase the particle transfer process. The turbulence created by these particles near the wall declines the thermal boundary layer thickness. However, the presence of these particles decreases the fluid flow close to the wall and reduces the velocity gradient in the zone. The heat transfer enhancement depends on how intense each of these two factors can be influential. Findings indicate that when the flow is at Re = 20000, the heat transfer rate rises when the magnetic field is employed; however, at Reynolds more than 20000, applying the magnetic field decreases the heat transfer rate compared to the non-porous channel. Thus, the magnetic field boosts the heat transfer rate for low Reynolds numbers only since the magnetic particles are more likely to transfer and produce turbulence in thermal boundary layers in low velocities.

Fig. 9a is dedicated to the variation of the average heat transfer coefficient in terms of nanofluid volume fraction for different *S* at $\beta = 0.5$ Tesla for boundary arrangement. The maximum heat transfer enhancement is approximated to be 3–5% for the case where the porous media's thickness is 0.6. The nanofluid and magnetic field effect on heat transfer is evaluated, and the data are shown in Fig. 9c and b and . The findings indicate that the heat transfer of the central arrangement is greater than the boundary arrangement for all cases.

Fig. 10a and b demonstrate the Nusselt number change with volume fraction for various cross-section shapes at Re = 20000, Da = 1E-4, and ε = 0.8. The graphs indicate that changing the porous media's cross-section shape reduces the heat transfer compared to the homogenous cylindrical porous layer. Regarding Fig. 10a, the amount of the decline in heat transfer is approximated to be 21%, 28.4%, and 13.6% for cases A, B, and C, respectively, when the thickness is 0.2. The heat transfer is reduced by 21.6%, 29.04%, and 14.3% for cases A, B, and C when the thickness is 0.6. The reason for this behavior is that reducing the contact surface between fluid and solid reduces heat transfer compared to the base state (i.e., the homogenous cylindrical porous layer). When the fins are twisted, the reduction of heat transfer is lower, mainly due to the slight difference in the flow pattern and the creation of the secondary flow. Increasing the volume fraction of the nanofluid improves the heat transfer in all cases. The magnetic field effect on thermal performance with the intensity of 0.5 T is studied specifically for Case C, and the results are shown in Fig. 10c. Regarding Fig. 10c, the heat

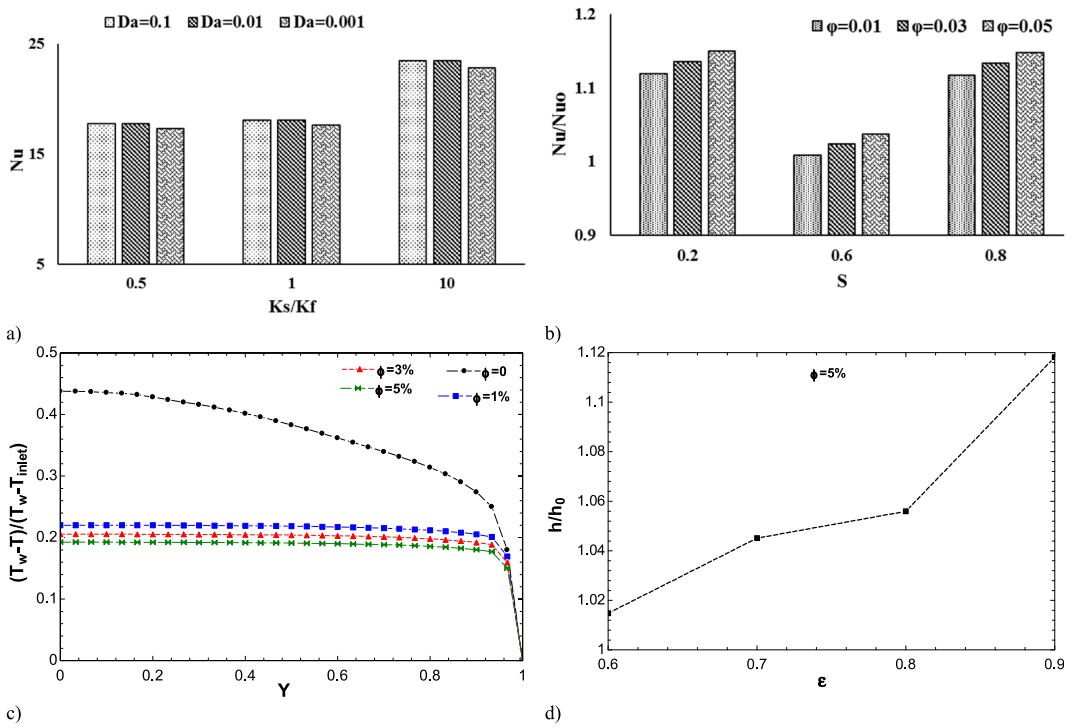

Fig. 7. a) The efficacy of ratio of thermal conductivity coefficient on the Nusselt number, b) the Relative Nusselt number ratio in terms of the thickness of the porous media, c) Variation of the dimensionless temperature for various volume fractions for boundary arrangements at Da = 1E-4, ε = 0.8, and Re = 20000, and d) Relative convective heat transfer with various porosities ∅ = 5% and Re = 20000.

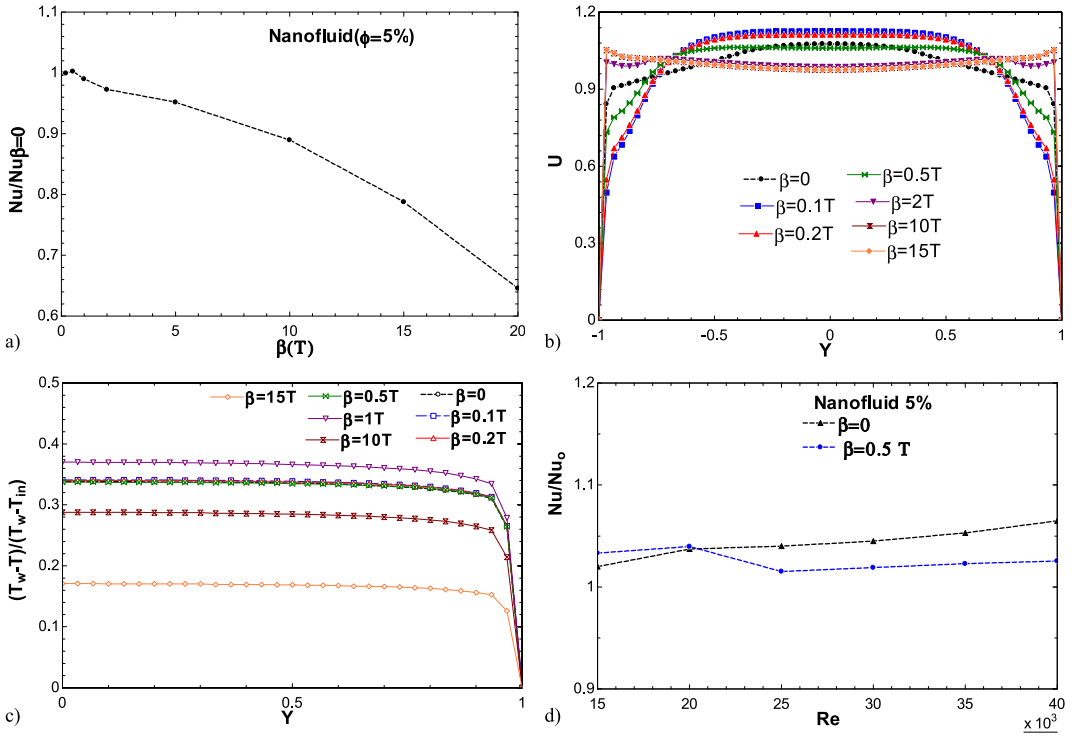

Fig. 8. a) variation of relative Nusselt number with magnetic field intensity, b) velocity, and c) variation of dimensionless temperature for various magnetic field intensities for boundary arrangement at Da = 1E-4, ε = 0.8, Re = 20000 and ∅ = 5%.

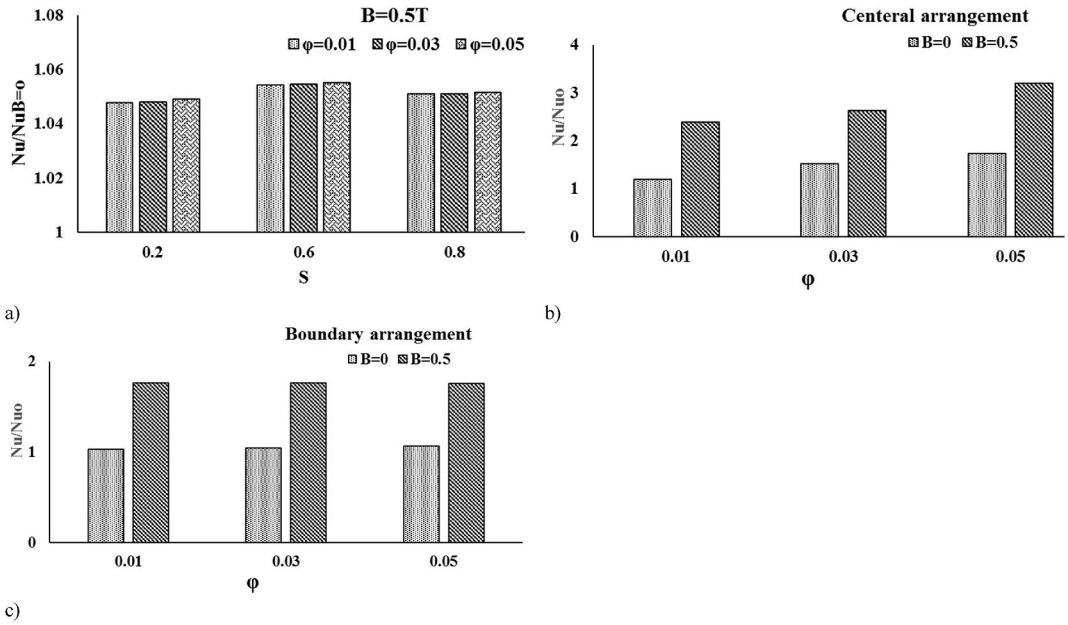

Fig. 9. a) variation of relative Nusselt number with the thickness of porous media and volume fractions at B = 0.5 T for boundary arrangement with and without magnetic field, b) for central arrangement, and c) boundary arrangement at Da = 1E-4, ε = 0.8, Re = 20000.

transfer is increased by approximately 18.1%, 18.7%, and 33.4% for volume fractions equal 1%, 3%, and 5%, respectively, when *S* is 0.2. The heat transfer rises by 18%, 18.4%, and 31.9% when *S* is 0.6 for the same order of volume fractions. As shown in Fig. 10d&e, the application of a magnetic field influences the heat transfer positively. The rise in heat transfer is approximated to be 24%, 8%, and 9% for cases A, B, and C, respectively, when the thickness is 0.2, and it is estimated to be 22%, 4.1%, and 10.9% for the same order of cases.

5. Conclusion

The current paper has explored the effect of porous media, nanofluid, and magnetic field on heat transfer of a circular channel. Two arrangements are assumed for the porous region in this problem; the central arrangement in which the porous zone is situated in the channel's core and the boundary arrangement where the porous media is affixed to the channel's wall. The research involves a 3D simulation with the help of FVM. The multiphase model is used to simulate the nanofluid in numerical simulation. The thermal conductivity ratio in the porous medium, volume fraction of nanofluid, Darcy number and magnetic field are set to 0.5-1,0-0.05, 0–0.1 and 0-15 T, respectively. The highlights of the study are summarized as follows:

- The efficacy of various porous placements on thermal performance has been investigated. The results present a critical thickness of porous media for both arrangements. Decreasing Darcy number increases Nusselt number. The heat transfer rate is estimated to increase by 32% when the thermal conductivity ratio (K_s/K_f) is changed from 0.5 to 10. Increasing the volume fraction increases the average heat transfer coefficient regardless of the porous region thickness. The minimum rise of the convective heat transfer coefficient occurs when the porous media's non-dimensional thickness is 0.6.
- The magnetic field effect on the thermal behavior of a partially filled pipe with porous and nanofluid has been examined. The average convective heat transfer rises when the magnetic field intensity is increased up to 0.5 T. Then it falls following the further increment of the magnetic field intensity. The magnetic field causes the heat transfer rate to improve at low Reynolds numbers only; Because the magnetic particles are more likely to transfer and produce turbulence in thermal boundary layers in low velocities. Based on the findings, the maximum heat transfer enhancement is approximated to be 3–5% for the case where the non-dimensional thickness of the porous media is 0.6.
- The variation of Nusselt number near the wall with various volume fractions of nanofluid for three cross-section shapes has been studied. Changing the porous media's cross-section shape reduces the heat transfer compared to the homogenous cylindrical porous layer. Geometry B has the minimum decline in heat transfer rate between the studied cases. The most significant reasons are the disorganized shape and twisting feature of the fins through the channel, resulting in turbulence in the flow.

Author statement

S.D. Farahani:Conceptualization, Methodology, Software, analysis, writing, editing, advisor. **M.Amiri**: Methodology, Software, analysis, writing. **B.K.Majd**: Software, analysis, writing. **A.Mosavi**: writing.

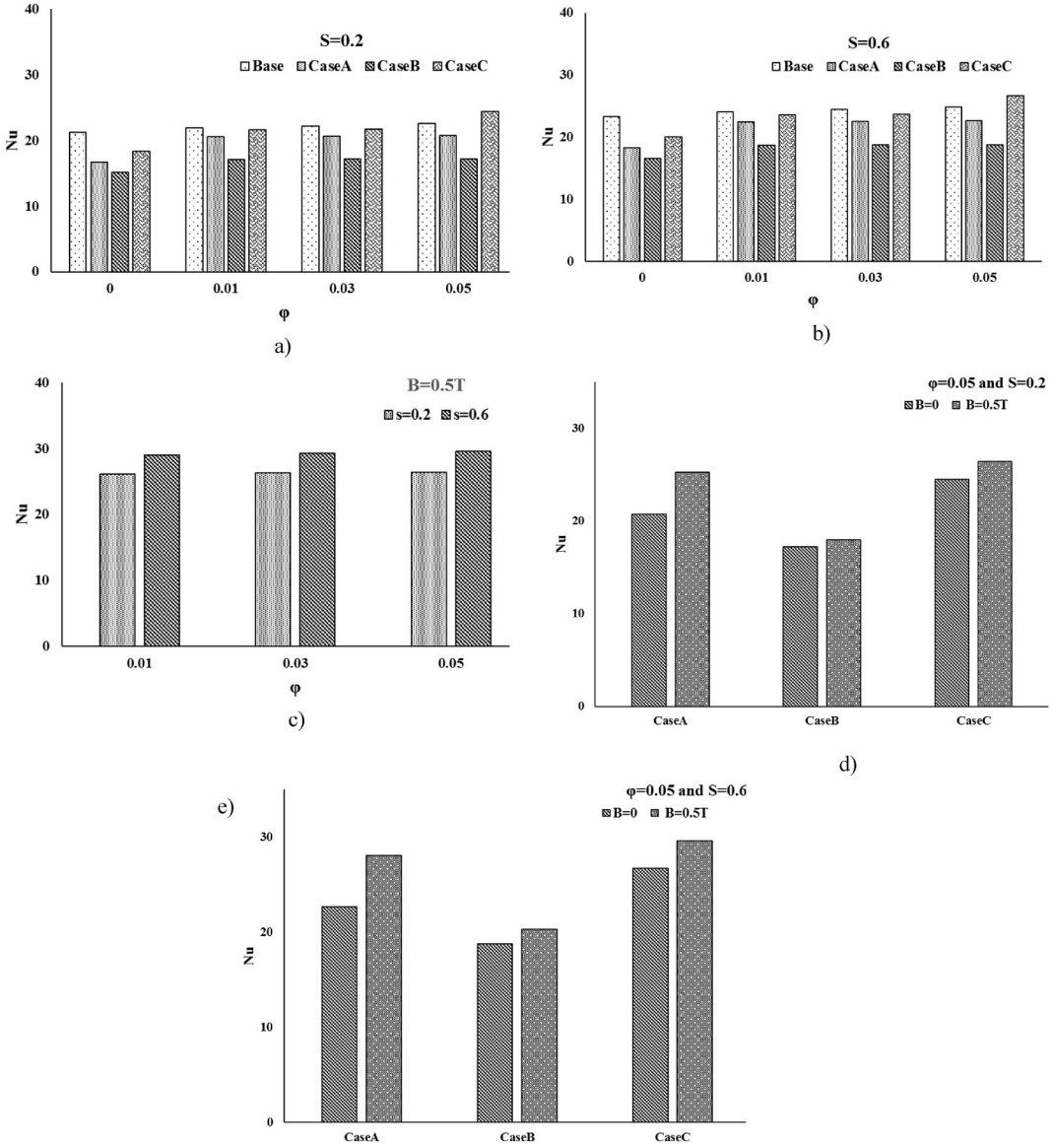

Fig. 10. a) and b) The effect of shape in porous media in boundary arrangement on Nusselt number with different volume fractions, c) the effect of magnetic field on heat transfer of case C for $\beta = 0.5Tesla$, d) and e) Comparison of the three geometries with and without the magnetic field.

Declaration of competing interest

The authors declare that they have no known competing financial interests or personal relationships that could have appeared to influence the work reported in this paper.

References

[1] M.M.M. Salih, O.R. Alomar, H.N.S. Yassien, Impacts of adding porous media on performance of double-pass solar air heater under natural and forced air circulation processes, Int. J. Mech. Sci. 210 (2021), 106738.
[2] D.A. Nield, A. Bejan, Convection in Porous Media, Springer, 2006.
[3] T. Tong, E. Subramanian, A boundary-layer analysis for natural convection in vertical porous enclosures—use of the Brinkman-extended Darcy model, Int. J. Heat Mass Tran. 28 (3) (1985) 563–571.
[4] P. Nithiarasu, K. Seetharamu, T. Sundararajan, Natural convective heat transfer in a fluid saturated variable porosity medium, Int. J. Heat Mass Tran. 40 (16) (1997) 3955–3967.
[5] C. Beckermann, S. Ramadhyani, R. Viskanta, Natural Convection Flow and Heat Transfer between a Fluid Layer and a Porous Layer inside a Rectangular Enclosure, 1987.
[6] X. Chen, P. Yu, Y. Sui, S. Winoto, H. Low, Natural convection in a cavity filled with porous layers on the top and bottom walls, Transport Porous Media 78 (2) (2009) 259–276.
[7] T. Tong, E. Subramanian, Natural convection in rectangular enclosures partially filled with a porous medium, Int. J. Heat Fluid Flow 7 (1) (1986) 3–10.

[8] C. Beckermann, R. Viskanta, S. Ramadhyani, Natural convection in vertical enclosures containing simultaneously fluid and porous layers, J. Fluid Mech. 186 (1988) 257–284.
[9] S. Baragh, H. Shokouhmand, S.S.M. Ajarostaghi, M. Nikian, An experimental investigation on forced convection heat transfer of single-phase flow in a channel with different arrangements of porous media, Int. J. Therm. Sci. 134 (2018) 370–379.
[10] M.E. Nimvari, N.F. Jouybari, Investigation of turbulence effects within porous layer on the thermal performance of a partially filled pipe, Int. J. Therm. Sci. 118 (2017) 374–385.
[11] H. Shokouhmand, P. Bagherzade, M. Fazli, A. Shomali, Thermal dispersion effects on heat transfer of laminar gas flow in a microtube filled with porous medium, Int. J. Therm. Sci. 122 (2017) 281–291.
[12] C. Peng, T. Ming, Y. Tao, Thermal and hydraulic performances of a tube filled with various thermal conductivities of porous media, Int. J. Heat Mass Tran. 81 (2015) 784–796.
[13] Z.-J. Zheng, M.-J. Li, Y.-L. He, Optimization of porous insert configurations for heat transfer enhancement in tubes based on genetic algorithm and CFD, Int. J. Heat Mass Tran. 87 (2015) 376–379.
[14] M. Dehghan, M.S. Valipour, S. Saedodin, Temperature-dependent conductivity in forced convection of heat exchangers filled with porous media: a perturbation solution, Energy Convers. Manag. 91 (2015) 259–266.
[15] B. Wang, Y. Hong, X. Hou, Z. Xu, P. Wang, X. Fang, X. Ruan, Numerical configuration design and investigation of heat transfer enhancement in pipes filled with gradient porous materials, Energy Convers. Manag. 105 (2015) 206–215.
[16] S. Nazari, R. Ellahi, M. Sarafraz, M.R. Safaei, A. Asgari, O.A. Akbari, Numerical study on mixed convection of a non-Newtonian nanofluid with porous media in a two lid-driven square cavity, J. Therm. Anal. Calorim. 140 (3) (2020) 1121–1145.
[17] M.H. Esfe, S. Esfandeh, E. Hosseinizadeh, Nanofluid flooding in a randomized heterogeneous porous media and investigating the effect of capillary pressure and diffusion on oil recovery factor, J. Mol. Liq. 320 (2020), 113646.
[18] S. Maaref, A. Kantzas, S.L. Bryant, The effect of water alternating solvent based nanofluid flooding on heavy oil recovery in oil-wet porous media, Fuel 282 (2020), 118808.
[19] C. Liu, M. Pan, L. Zheng, P. Lin, Effects of heterogeneous catalysis in porous media on nanofluid-based reactions, Int. Commun. Heat Mass Tran. 110 (2020), 104434.
[20] A.R. Gheynani, O.A. Akbari, M. Zarringhalam, G.A.S. Shabani, A.A. Alnaqi, M. Goodarzi, D. Toghraie, Investigating the effect of nanoparticles diameter on turbulent flow and heat transfer properties of non-Newtonian carboxymethyl cellulose/CuO fluid in a microtube, Int. J. Numer. Methods Heat Fluid Flow 11 (4) (2019) 112–132.
[21] A.A. Al-Rashed, L. Kolsi, H.F. Oztop, A. Aydi, E.H. Malekshah, N. Abu-Hamdeh, M.N. Borjini, 3D magneto-convective heat transfer in CNT-nanofluid filled cavity under partially active magnetic field, Phys. E Low-dimens. Syst. Nanostruct. 99 (2018) 294–303.
[22] M. Sheikholeslami, M. Rashidi, D. Ganji, Effect of non-uniform magnetic field on forced convection heat transfer of Fe3O4–water nanofluid, Comput. Methods Appl. Mech. Eng. 294 (2015) 299–312.
[23] M. Sheikholeslami, Z. Ziabakhsh, D. Ganji, Transport of Magnetohydrodynamic nanofluid in a porous media, Colloid. Surface. Physicochem. Eng. Aspect. 520 (2017) 201–212.
[24] F. Selimefendigil, H.F. Öztop, MHD Pulsating forced convection of nanofluid over parallel plates with blocks in a channel, Int. J. Mech. Sci. 157 (2019) 726–740.
[25] H. Arasteh, R. Mashayekhi, D. Toghraie, A. Karimipour, M. Bahiraei, A. Rahbari, Optimal arrangements of a heat sink partially filled with multilayered porous media employing hybrid nanofluid, J. Therm. Anal. Calorim. 137 (3) (2019) 1045–1058.
[26] W. He, D. Toghraie, A. Lotfipour, F. Pourfattah, A. Karimipour, M. Afrand, Effect of twisted-tape inserts and nanofluid on flow field and heat transfer characteristics in a tube, Int. Commun. Heat Mass Tran. 110 (2020), 104440.
[27] P. Barnoon, D. Toghraie, F. Eslami, B. Mehmandoust, Entropy generation analysis of different nanofluid flows in the space between two concentric horizontal pipes in the presence of magnetic field: single-phase and two-phase approaches, Comput. Math. Appl. 77 (3) (2019) 662–692.
[28] S.D. Farahani, A.D. Farahani, E. Hajian, Effect of PCM and porous media/nanofluid on the thermal efficiency of microchannel heat sinks, Int. Commun. Heat Mass Tran. 127 (2021), 105546.
[29] S.D. Farahani, A.D. Farahani, F. Tayebzadeh, A. Mosavi, Melting of non-Newtonian phase change material in a finned triple-tube: efficacy of non-uniform magnetic field, Case Stud. Therm. Eng. (2021), 101543.
[30] R.A. Silva, M.J. de Lemos, Turbulent flow in a channel occupied by a porous layer considering the stress jump at the interface, Int. J. Heat Mass Tran. 46 (26) (2003) 5113–5121.